PCCP

Length Dependence thermal conductivity of Zinc-Selenide (ZnSe) and Zinc Telluride (ZnTe)- A combined first principles and Frequency Domain Thermoreflectance (FDTR) study

Journal:	*Physical Chemistry Chemical Physics*
Manuscript ID	CP-ART-08-2022-003612.R1
Article Type:	Paper
Date Submitted by the Author:	25-Oct-2022

Complete List of Authors:	Muthaiah, Rajmohan; University of Oklahoma, School of Aerospace and Mechanical Engineering Annam, Roshan Sameer; University of Oklahoma, Aerospace and Mechanical Engineering Tarannum, Fatema; University of Oklahoma, Aerospace and Mechanical Engineering Gupta, Ashish; Oklahoma State University Garg, Jivtesh; University of Oklahoma, School of Aerospace and Mechanical Engineering Arafin, Shamsul; The Ohio State University, Electrical and Computer Engineering

Length Dependence thermal conductivity of Zinc-Selenide (ZnSe) and Zinc Telluride (ZnTe)- A combined first principles and Frequency Domain Thermoreflectance (FDTR) study

Rajmohan Muthaiah[a], Roshan Sameer Annam[a], Fatema Tarannum[a], Ashish Kumar Gupta[b], Jivtesh Garg[a], Shamsul Arafin[c]

a. School of Aerospace and Mechanical Engineering, University of Oklahoma, Norman, OK-73019, USA
b. Department of Mechanical and Aerospace Engineering, Oklahoma State University, Stillwater, OK 74078, USA
c. Department of Electrical and Computer Engineering, Ohio State University, Columbus, OH 43210, USA

Abstract:

In this study, we report the length dependence of thermal conductivity (k) of zinc-blende Zinc-Selenide (ZnSe) and Zinc Telluride (ZnTe) for length scales between 10 nm and 10 μm using first-principles computations based on density-functional theory. k value of ZnSe is computed to decrease significantly from 22.9 W/m-K to 1.8 W/m-K as the length scale is diminished from 10 μm to 10 nm. k value of ZnTe is also observed to decrease from 12.6 W/m-K to 1.2 W/m-K for the same decrease in length. We also measured the k of bulk ZnSe and ZnTe using Frequency Domain Thermoreflectance (FDTR) technique and observed a good agreement between FDTR measurements and first principles calculations for the bulk ZnSe and ZnTe. Understanding of thermal conductivity reduction at nanometer length scales provides an avenue to incorporate nanostructured ZnSe and ZnTe for thermoelectric applications.

Keywords: Zinc Selenide, Zinc Telluride, Frequency Domain Thermo-reflectance, Nanostructures, First Principles calculations, thermal management system and thermoelectric.

Introduction:

With the development of improved manufacturing capabilities, the field of microelectronics has advanced significantly[1-3], leading to a significant reduction in the sizes of the transistors being used as predicted by Moore's Law[4]. As the length scale of the materials approach nanometers[5], thermal conductivity exhibited by these materials changes significantly[6-

16].Reduction in size leads to a significant drop in their thermal conductivity[17], leading to a rise in working temperatures in electronic applications. This phenomenon diminishes reliability and performance in microelectronics[18]. Hence, effective thermal management has received significant attention as an area of concern in the design of modern microelectronics [7, 9, 12, 15, 19, 20]. Low thermal conductivity can also be beneficial for applications such as thermoelectrics where lower lattice thermal conductivity minimizes heat loss through lattice vibrations, improving the energy conversion efficiency. Many techniques such as Scanning Thermal Microscopy (SThM)[21], Time Domain Thermoreflectance (TDTR)[22-24] and Frequency Domain Thermoreflectance (FDTR)[25] have been used to understand and gain insights into the transport phenomena at nanometer length scales.

Zinc Chalcogenides (ZnX, X=S, Se and Te) are II-VI wide band gap semiconductors that crystallize in zinc-blende structure[26-31] and are mainly studied for catalysis[32], electronic[33, 34], structural[34], opto-electronic[35], thermal[29, 36] and thermoelectric properties[37]. In recent times, thin films and nanostructured ZnSe have been widely investigated[28, 37], however, their thermal conductivity dependence on size is unknown. In this work, we report the bulk and length dependent lattice thermal conductivity (k) of ZnSe and ZnTe by solving phonon Boltzmann transport equation (PBTE) coupled with harmonic and anharmonic interatomic force interactions derived from density-functional theory[38-40]. At 300 K, our first-principles estimated k values of isotopically pure ZnSe and ZnTe are 25.4 W/m-K and 15.2 W/m-K respectively. The k values of isotopically disordered ZnSe and ZnTe are 23.2 W/m-K and 14.2 W/m-K respectively. Based on good agreement with the previous works[41], we computed length dependent k of ZnSe and ZnTe by including Casimir scattering[42].

We first discuss the details of computation of bulk and length dependent k of ZnSe and ZnTe using first principles calculations and details of FDTR setup for measurement of k of polycrystalline ZnSe and ZnTe [25, 43-46] followed by results and discussion. We discuss the phonon dispersions, phonon group velocities, phonon scattering rates, phonon meanfreepaths and mode dependent contribution of transverse acoustic (TA), longitudinal acoustic (LA) and optical phonons for both ZnSe and ZnTe, as well as the length dependence and meanfreepath accumulation of k for the two materials.

We also provide brief description of FDTR which is a non-destructive, non-contact[45] method of measuring the thermal properties of a material. This experimental method utilizes optical pump-probe technique which comprises of a pump laser, which provides a sinusoidal heat signal to material under study and probe laser which measures the corresponding phase lag of the temperature relative to the heat signal provided by the pump laser. In FDTR, the pump laser beam is frequency modulated and the measurement is done across a range of frequencies. The frequency of modulation is supplied using a signal generator[43, 46], where in this case, the Lock-In amplifier[43, 46] has the capability of generating input signals of up to 50MHz and the frequency range utilized for this measurement was 2kHz – 50MHz. The sample is coated with a thin layer (~100nm) of gold of high coefficient of thermoreflectance at the probe beam wavelength (532nm). The measurement is performed by fitting the measured phase lag, induced by the material $\varphi = \varphi_{pump} - \varphi_{probe}$ to the phase lag that is predicted using a 2D heat conduction model, which involves various input parameters such as transducer thickness, thermal properties of the thin film metal transducer and the effective spot size of the probe beam that was measured during the experiment. Various combinations of thermal and geometrical properties can be extracted with great confidence from this measurement. This measurement is also useful for identifying the isotropy /anisotropy of the materials[47-50]. FDTR is a very versatile measurement technique and can be used to measure the thermal properties of a wide range of material systems such as solids[22, 25, 46, 51, 52], liquids[46, 53, 54], thin films[46, 55-57], and the thermal conductance of interfaces[58-61].

Computational Details:

Thermal conductivity in this work is computed by solving the phonon Boltzmann transport equation (PBTE) described below,

$$-\boldsymbol{c}(\boldsymbol{q}s)\cdot\nabla T\left(\frac{\partial n_{\boldsymbol{q}s}}{\partial T}\right)+\frac{\partial n_{\boldsymbol{q}s}}{\partial T}|_{scatt}=0$$

where, $n_{\boldsymbol{q}s}$ is the population of phonon mode with wave-vector $\boldsymbol{q}$ and polarization s, T is temperature and $\boldsymbol{c}(\boldsymbol{q}s)$ is the phonon group velocity computed using $\boldsymbol{c}(\boldsymbol{q}s)=\partial\omega_{\boldsymbol{q}s}/\partial\boldsymbol{q}$, ($\omega_{\boldsymbol{q}s}$ represents the frequency of phonon mode $\boldsymbol{q}s$). The equation represents a balance between change in phonon population due to temperature gradient (first term in the equation) and change in

population due to scattering (second term). In this work, PBTE is solved exactly for phonon population using QUANTUM ESPRESSO thermal2 code. Knowledge of perturbed phonon populations allows computation of thermal conductivity.

The only ingredients required to compute all phonon properties involved in PBTE are the second order (harmonic) and third-order (anharmonic) interatomic force interactions. These force interactions were derived accurately in this work from first-principles. Harmonic force interactions are needed to compute phonon frequencies, group velocities and populations while anharmonic force interactions enable computation of phonon scattering. Harmonic interactions were derived using the PHONON code[62], while anharmonic interactions were derived using D3Q package[63, 64], both within the QUANTUM ESPRESSO density-functional theory (DFT) code.

All the first principles calculations were performed using plane-wave based QUANTUM ESPRESSO[65] package. We used local density approximation (LDA)[66] and norm-conserving pseudopotentials for electronic calculations. Calculations were carried out with plane-wave energy cut-off of 80 Ry and Monkhorst-Pack[67] *k*-point mesh of 12 x 12 x 12 was used for integration over Brillouin zone. Crystal structure was relaxed until the total force acting on each atom diminished below 1e-5 eV/Å. Optimized lattice constants of *Zinc-blende* ZnSe and ZnTe were determined to be a=5.6 Å and a=6.138 Å. Dynamical matrices were computed on 8 x 8 x 8 **q**-grid mesh. Inverse Fourier transform was used to convert these matrices in **q**-space into 2^{nd} order force constants (harmonic) in real space on an 8 x 8 x 8 supercell. Anharmonic (3^{rd} order) interatomic force constants were similarly first computed on 4 x 4 x 4 **q**-grid using QUANTUM ESPRESSO D3Q[62-64] package and then inverse-Fourier transformed to obtain the force constants in real space. Lattice thermal conductivity is calculated by solving Peierls-Boltzmann transport equation (PBTE)[62, 64, 68]iteratively within QUANTUM ESPRESSO thermal2 code[62-64] with 30 x 30 x 30 **q**-mesh. Casimir scattering[42] is imposed for length dependence *k* calculations.

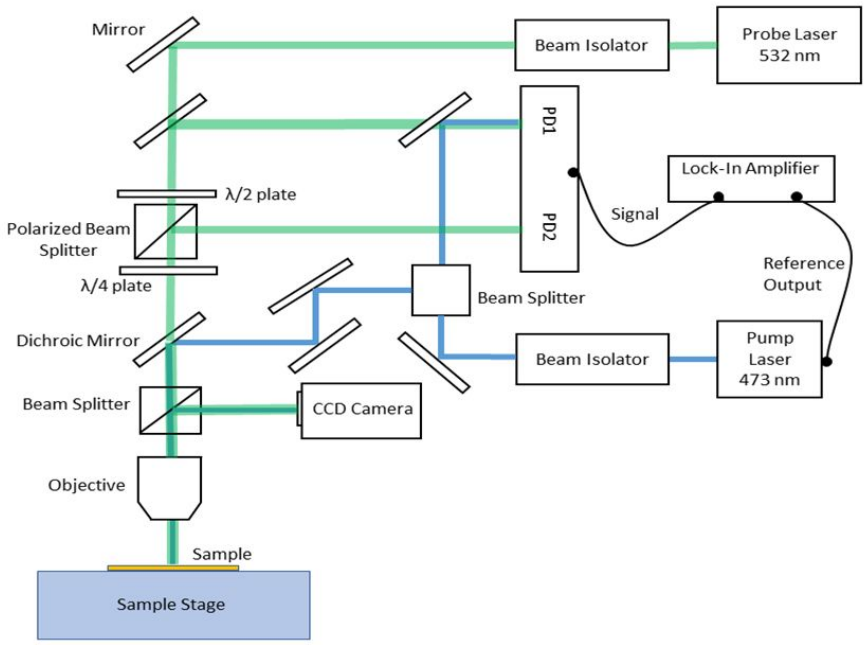

Figure 1. Frequency Domain Thermoreflectance (FDTR) experimental setup

Experimental Setup[45, 46]:

The FDTR system setup consists of two 20mW continuous-wave free space diode lasers (Coherent OBIS), namely, the pump laser (blue) which works at the wavelength of 473 nm and the probe laser (green) which operates at a wavelength of 532 nm. The pump laser is modulated digitally with the help of output reference of the Lock-In amplifier (Zurich Instruments HF2LI). The driving signal used for pump laser modulation is a sinusoidal signal with a 2V peak to peak voltage and frequencies ranging from 2 kHz to 50 MHz. The beams from these lasers pass through optical isolators (Thorlabs IO-5-532-HP for 532nm, Thorlabs IO-3-780-HP for 785 nm), which prevent any backscattering of laser beam into the aperture of the laser, thus protecting the laser from output power instabilities. The setup also utilizes mirrors to appropriately direct the laser beam in the desired direction. Using a beam splitter, 1% of the pump laser beam is directed towards a photodetector which records the phase of the pump beam, referred to as pump phase or φ_{pump}. A dichroic mirror (Edmund Optics, hot mirror) reflects the pump beam onto the sample through the microscopic objective. This creates a periodic heat flux on the sample's surface with spot intensity being maximum in the middle and decaying towards the edges according to a Gaussian spatial distribution. Both the pump and probe beams are aligned coaxially, and the probe beam is used to measure the change in phase of the temperature response of the surface with respect to the phase

of the input heat signal. This is achieved by measuring the surface temperature through a measurement of the intensity of the reflected probe beam (the two are correlated through the fact that surface reflectivity is a function of surface temperature). Every sample whose thermal properties are measured using FDTR utilizes a thin film of metal, whose thickness is in the range of 80-100 nm. The metal film maximizes the coefficient of thermo-reflectance at the probe's operating wavelength. Balanced photodetection is implemented to improve the signal to noise ratios at the low frequencies of modulation for the pump laser. Balanced photodetector like

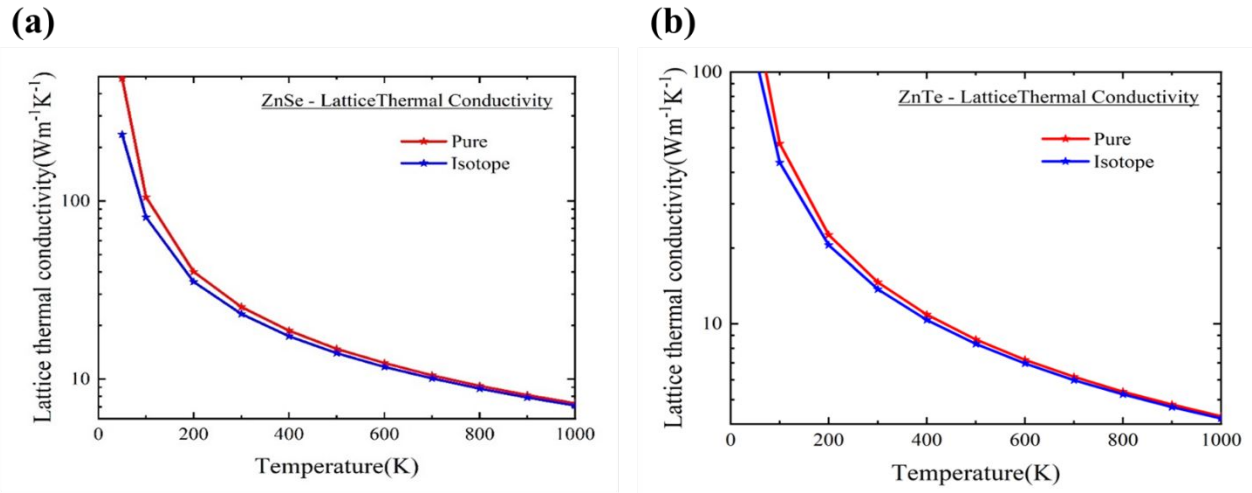

Figure 2. Lattice thermal conductivity of pure and naturally occurring a) ZnSe and b) ZnTe.

Thorlabs PDB415A is used, as it consists of two well matched photodiodes namely, PD1 and PD 2. A polarizing beam splitter (PBS) is utilized to split the probe beam into a pre-sample beam and a post-sample beam. The pre-sample beam is reflected into PD 2 as shown in the schematic (Figs. 1). The post-sample beam is reflected from the sample surface and reflected again using the dichroic mirror into PD 1. In order to reduce noise in the PD signal, the optical path lengths to PD 1 and PD 2 need to be matched. The noise minimization is achieved by delicately balancing the pre and post sample beams, by adjusting the half-wave plate. Another way of noise rejection that has been implemented is by letting the subtracted signal of PD 1 and PD 2 pass through a low noise transimpedance amplifier. This method helps eliminate noise from the probe beam, which is a common problem in the measurement. To prevent the thermal signal from getting overwhelmed by the backscattering of the pump beam, two band pass filters (FGB37) are used before the photodetectors.

The measurement of FDTR in our case works by comparing the phase lag of probe beam's post-sample beam (as discussed earlier) with respect to the phase of the periodic pump heat source. It is important to note that all the components within the experimental setup along with the path lengths traversed by both the pump and probe beams introduce a frequency-dependent phase shift to the signal which is denoted by φ_{ext}. This phase shift is accounted for by sampling 1% of the pump beam and directing it into the post-sample photodetector. φ_{ext} is then measured over a range of the modulation frequencies for the pump beam and is subtracted from the phase signal that has been measured, before fitting the measured data to a thermal model. In the setup, we also use a translation stage to adjust the sample height which keeps the sample in sharp focus i.e., the sample is in the depth of focus of the objective lens being used. This step is of utmost importance as a sharp image of a focused sample helps in the accurate determination of the spot size, which is a vital input parameter for the thermal model. The image of the sample being focused is obtained by using a CCD (charge-coupled device) camera.

The ZnSe and ZnTe bulk crystals were purchased from MTI Corporation. The gold pellet for the deposition of gold[45, 48, 69] thin film on bulk polycrystalline ZnSe was purchased from Kurt. JLesker Company (99% purity). We use Lesker Nano36 Evaporator thermal evaporator, (part of Microfabrication Research & Education Center at University of Oklahoma) to deposit 100nm of gold film. After this, the sample was placed carefully on a glass slide using double sided carbon tape, making it ready for measurement using FDTR.

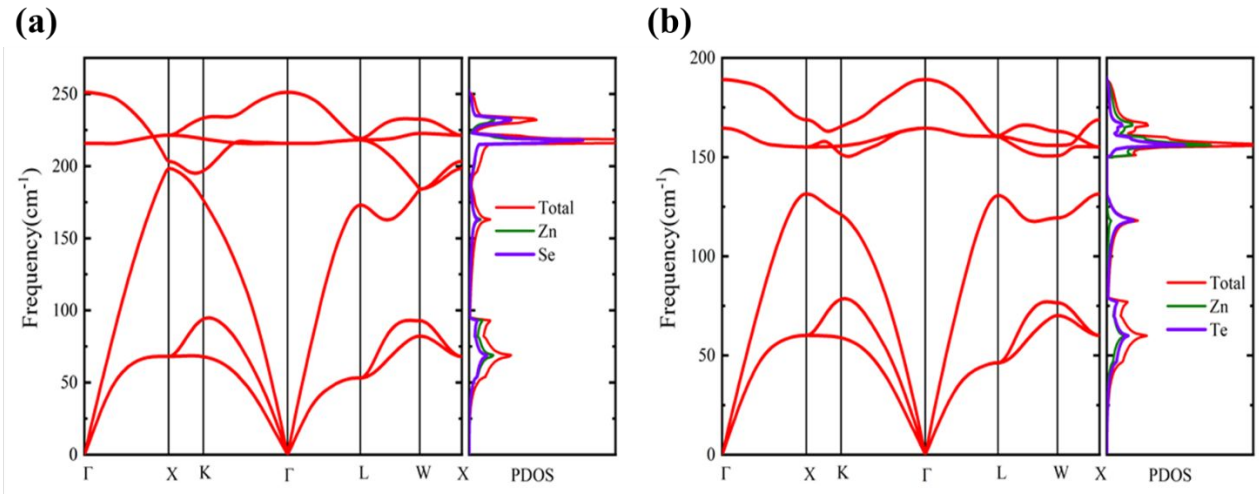

Figure 3. Phonon Density of States of a) ZnSe b) ZnTe

Results and Discussions:

Temperature dependent lattice thermal conductivity(k) of Zinc Selenide (ZnSe) and Zinc Telluride (ZnTe) derived from first-principles computations is shown in Figs. 2a and 2b respectively. At room temperature (300K), k of 23.2 W/m-K is computed for the naturally occurring ZnSe in close agreement with the previously reported experimental value [29]. Length dependent k of ZnSe nanostructures was computed from first principles calculations by imposing Casimir/boundary scattering[42] and is shown in Fig. 4a. Casimir boundary scattering was imposed by assuming the length to be the same in all three directions and thus relates to the case of a grain with similar dimensions in all directions. The length-dependent k value thus computed is isotropic in nature. k value of ZnSe is observed to decrease significantly from 22.9 W/m-K to 1.8 W/m-K as the length scale is diminished from 10 μm to 10 nm (Fig. 4a). Bulk k of ZnTe is computed to be 14.17 W/m-K for the naturally occurring case and is again in close agreement with the previously reported values[41]. k value of natural ZnTe is also observed to decrease significantly from 12.6 W/m-K to 1.2 W/m-K as the length scale is diminished from 10 μm to 10 nm (Fig. 4b). We investigated the phonon dispersion, phonon group velocity, phonon scattering rate and phonon mean free path in detail to explain these thermal conductivity results.

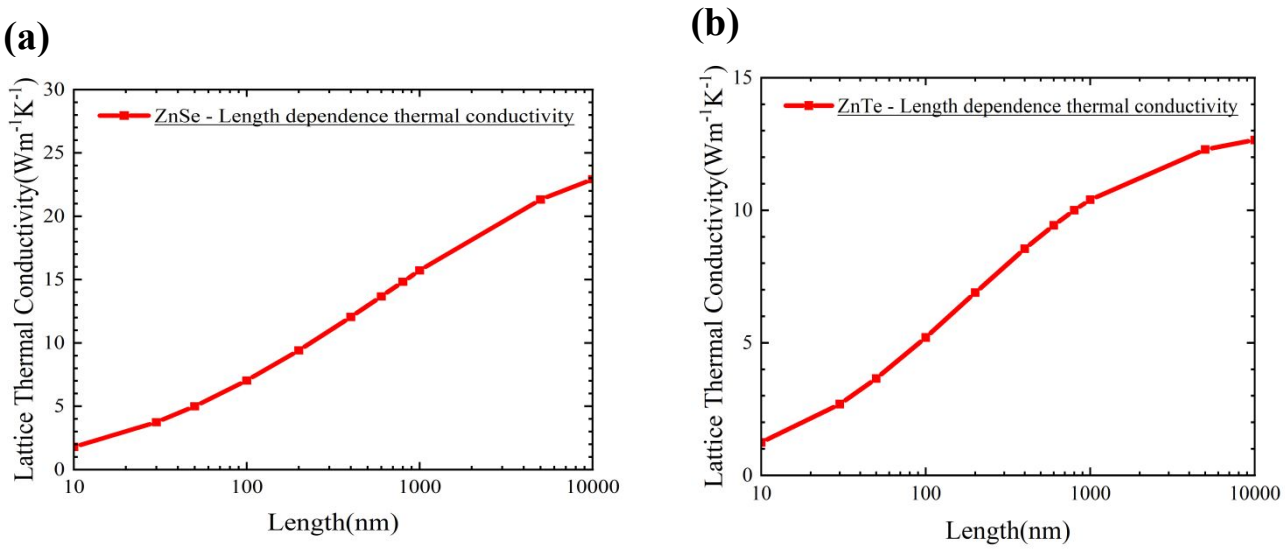

Figure 4. Length dependent thermal conductivity of isotopically disordered a) ZnSe b) ZnTe

We first compare the thermal conductivity accumulation (at 300 K) with respect to phonon mean freepath (MFP) in Figs. 5a and 5b for ZnSe and ZnTe respectively. Length dependence of *k* (shown in Figs. 4a and b) can be understood based on mean freepath accumulation of *k*. Fig. 5a shows that in ZnSe, phonons with mean freepath below 100 nm contribute ~8 W/m-K to overall *k*, which leads to a length dependent *k* of ~ 8 W/m-K at 100 nm length scale for ZnSe. Contributions of transverse acoustic (TA), longitudinal acoustic (LA) and optical phonons to overall thermal conductivity are shown in Figs. 6a and 6b for ZnSe and ZnTe respectively.

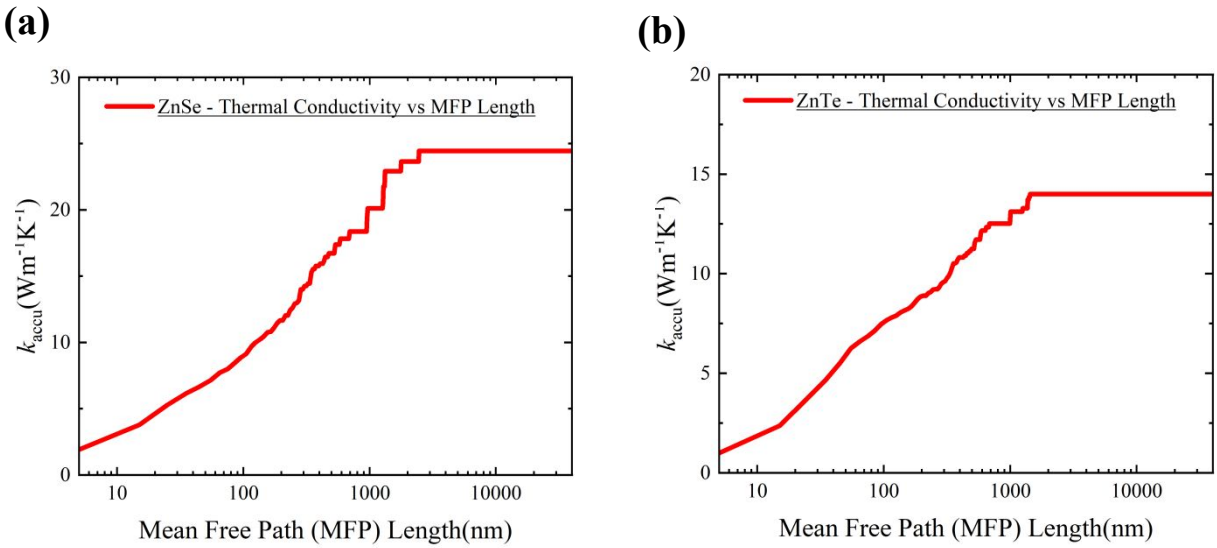

Figure 5. Mean free path length dependent thermal conductivity of isotopically disordered a) ZnSe b) ZnTe

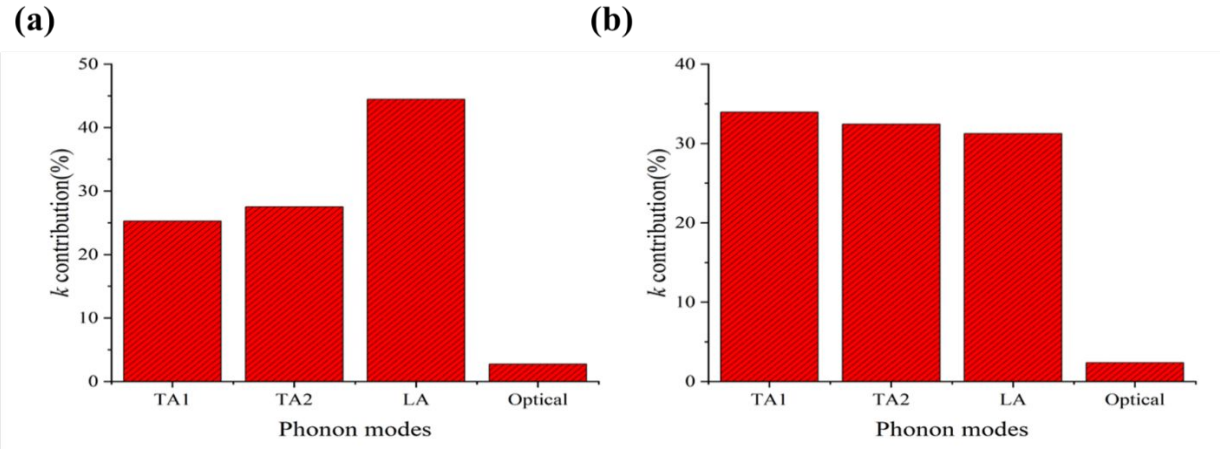

Figure 6. Thermal conductivity contribution from TA, LA and optical; phonon modes for a) ZnSe and b) ZnTe.

Phonon line widths (inverse of lifetimes) are shown in Figs. 7a and 7b and phonon group velocities are shown in Figs. 8a and 8b for ZnSe and ZnTe, respectively. In ZnSe, the contribution of LA phonons to overall thermal conductivity is higher than TA and optical phonons (Fig. 6a). This can be understood by noticing that LA phonons have higher phonon group velocities (Fig. 8a), and their scattering rates (Fig. 7a) are lower than TA phonons (in the low frequency range) in ZnSe.

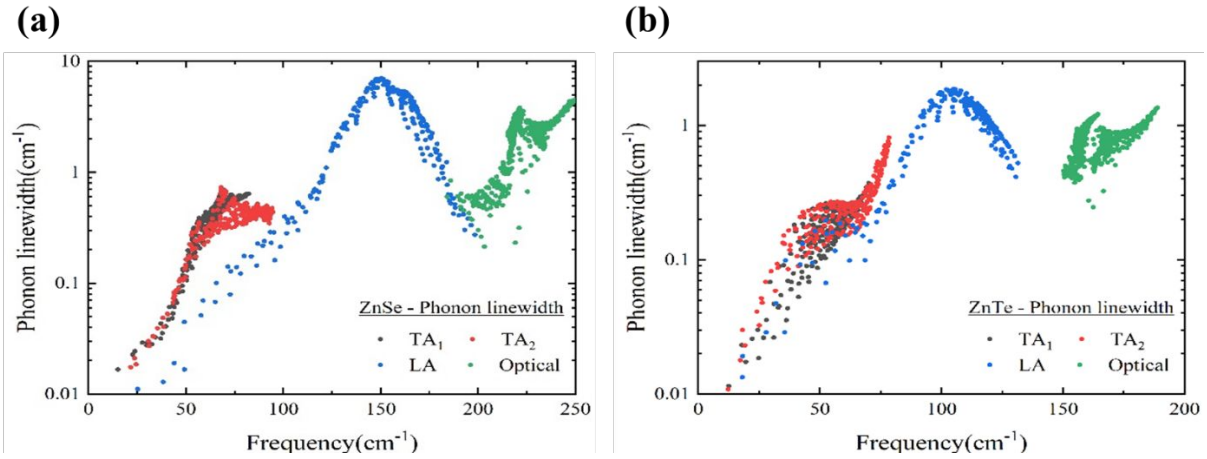

Figure 7. Phonon scattering rates of a) ZnSe b) ZnTe

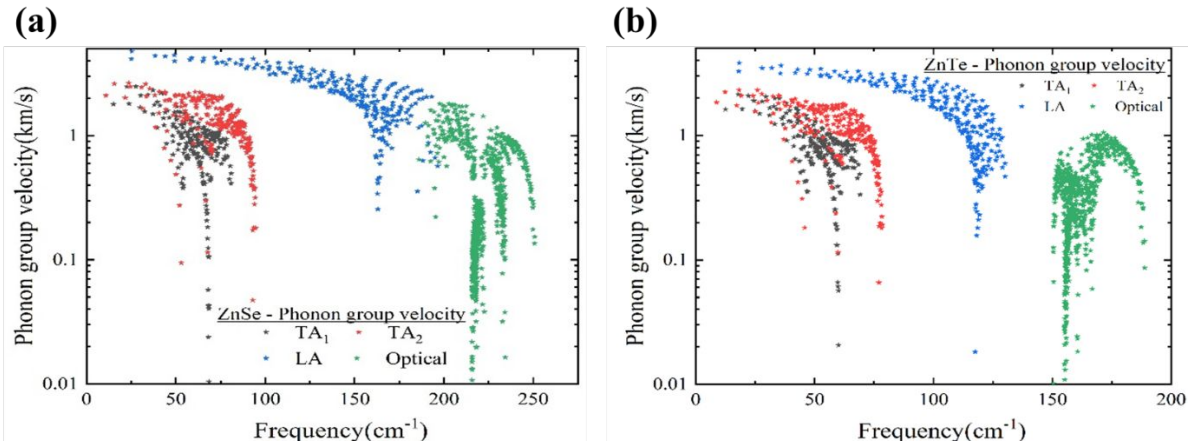

Figure 8: Phonon group velocities of a) ZnSe b) ZnTe

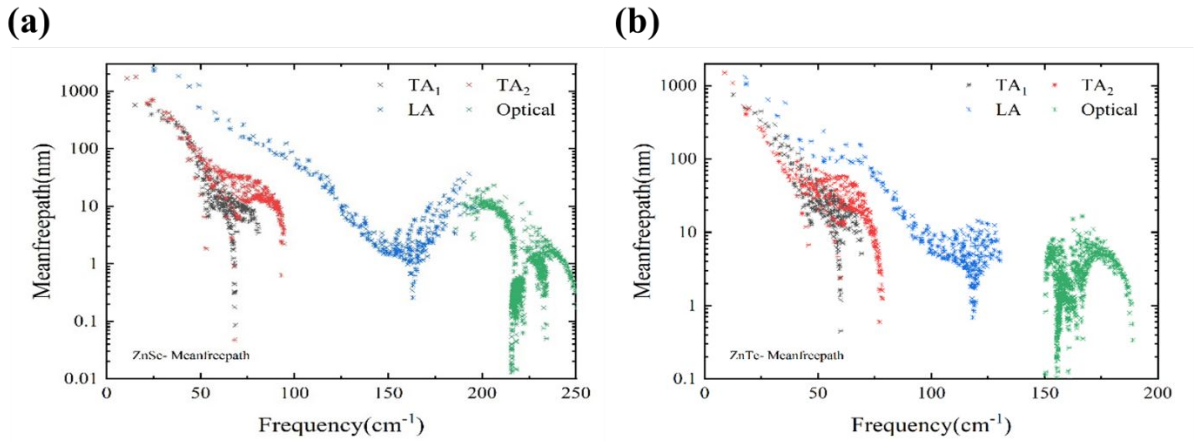

Figure 9. Phonon Mean free paths of a) ZnSe b) ZnTe

LA phonons contribute almost 44.5% to overall thermal conductivity in ZnSe. In case of ZnTe, the contribution of TA_1, TA_2 and LA phonons are ~34%, 32% and 31% respectively at 300 K.

FDTR Measurement: The experimentally measured thermal conductivity values of Zinc Selenide (ZnSe) and Zinc Telluride (ZnTe) using FDTR were ~17 W/m-K and 14 W/m-K respectively at room temperature. Comparing experimental thermal conductivity results from FDTR and theoretical results as shown in Figs. 4a and 4b, we can determine that the grain sizes of the ZnSe and ZnTe samples (obtained from the MTI Corp.) are in the range of 2μm to 10μm[71]. The measurement of thermal conductivities of polycrystalline ZnSe and ZnTe using FDTR is achieved by curve fitting method as explained in the experimental setup. The blue circles (in Fig. 10) represent the phase-lag data that has been measured using the FDTR setup. The frequency of lock-

in amplifier was set at 1MHz and the laser power of the pump and the probe lasers were set at 20mW and 5mW respectively for all samples measured in this work. The solid line represents the best fit curve, which is obtained by a 2D heat conduction mathematical model which utilizes known input parameters such as volumetric heat capacity of the gold film, gold film thermal conductivity, film thickness, volumetric heat capacity of the material under investigation, the thickness of the material under investigation and the laser spot size. The properties of gold film and its thickness are determined by depositing the gold film over a substrate with known properties, namely, fused Silica (k ~1 W/m-K) and Sapphire (k ~35 W/m-K).

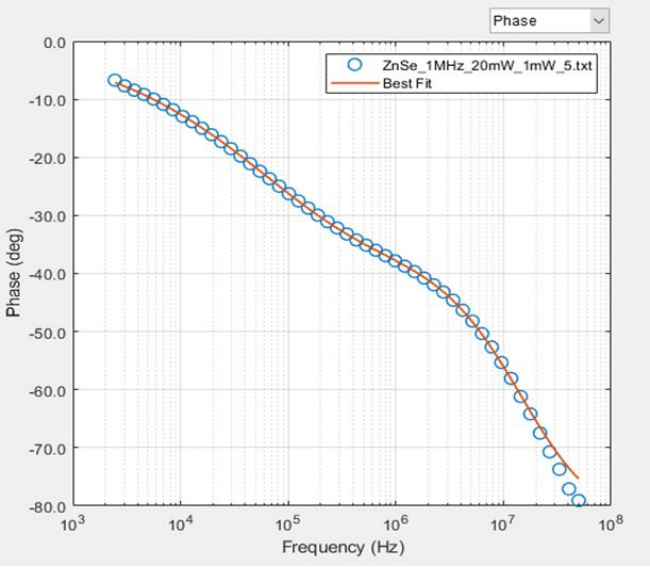

Figure 10. FDTR data for curve fitting analysis to calculate the thermal properties of ZnSe measured at a lock-in frequency of 1MHz along with pump and probe powers at 20 and 5mW respectively.

This results in accurate determination of the properties of the gold thin film. The volumetric heat capacities of ZnSe and ZnTe are obtained by multiplying the density (g/cm^3) and specific heat (J/Kg K). These details are available on the datasheet of the ZnSe and ZnTe on MTI Corporation's website[72]. The only unknown property in our study is the thermal conductivity of ZnSe and ZnTe, which leads to a single parameter fit.

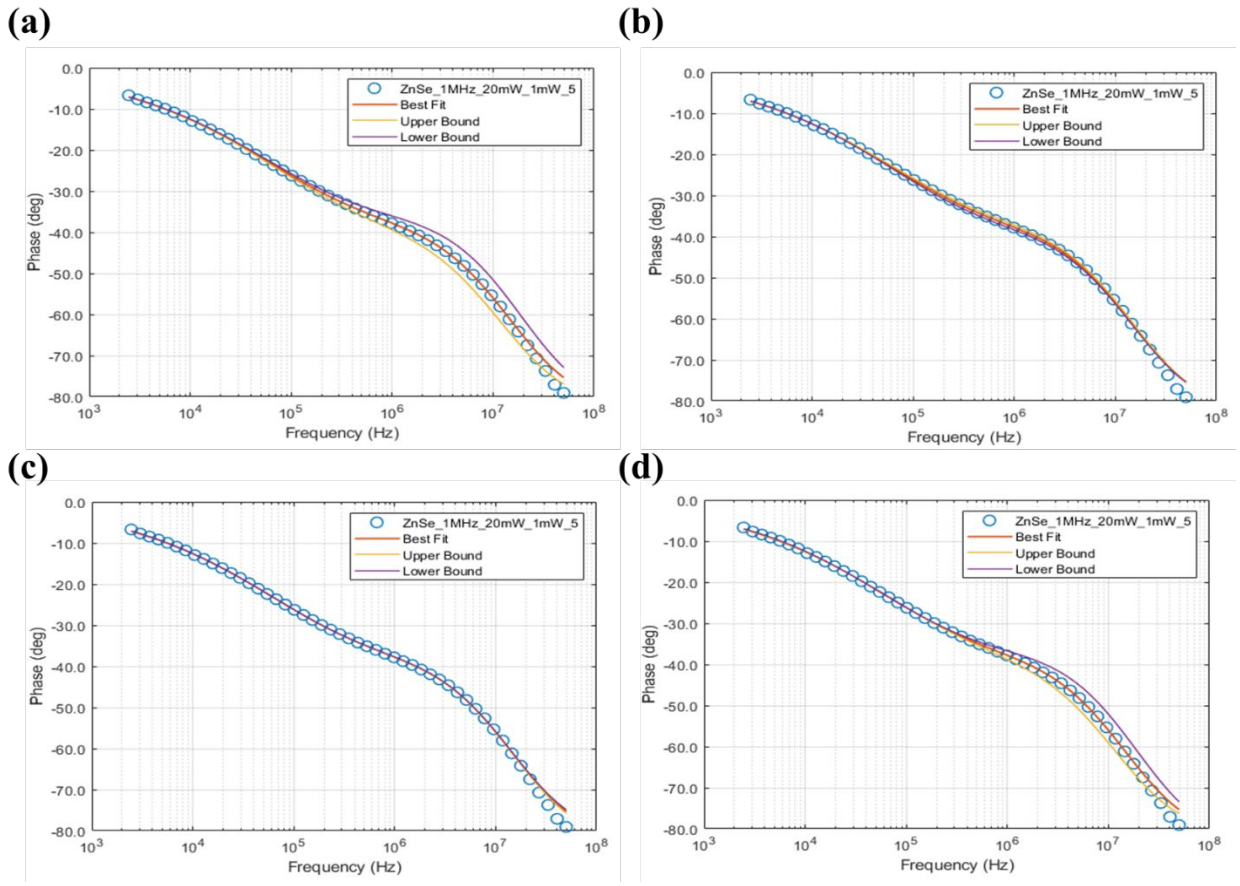

Figure 11. Sensitivity of phase-lag to a) gold volumetric heat capacity b) gold cross plane thermal conductivity c) gold in-plane thermal conductivity and d) thickness of gold film deposited on top of the ZnSe crystal.

For the measured thermal conductivity to be accurate, the measured data and the predicted phase-lag from heat conduction model should agree very well. As shown in Figs. 10, the best fit curve agrees very well with the measured phase-lag values (represented by blue circles). The figure is representative of the agreement between the measured phase data and the phase data generated using the mathematical model which utilizes the input parameters mentioned earlier in the section.

We next describe the sensitivity analysis which is important in ascertaining the accuracy of measured thermal conductivity values. Insensitive parameters can be fixed as input parameters in the model as they do not affect the curve fitting, and this reduces the number of free parameters to be fitted. Sensitive parameters are seen to have a significant difference in the upper and lower bound values of the phase lag measured in degrees (Figs. 11a, 11d), while insensitive parameters demonstrate small difference between these bounds (Figs. 11b, 11c). Figs. 11a, 11b and 11d show that the measurement is sensitive to gold thin film's volumetric heat capacity, gold's cross-plane thermal conductivity and its thickness (essential input parameters). Figs. 12a and 12b, show that the measurement is sensitive to the cross and in-plane thermal conductivity of bulk polycrystalline ZnSe. Figs. 13a and 13b represent another way of understanding sensitivity in terms of the phase difference values.

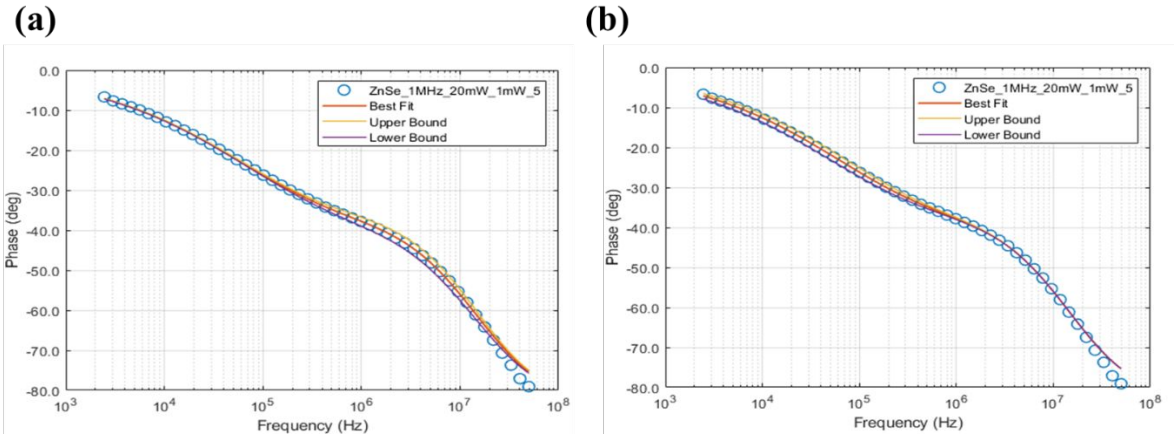

Figure 12. Sensitivity of a) Cross Plane b) In Plane thermal conductivity parameters of ZnSe Crystal

As seen in Fig. 13, the sensitivity analysis shown in Figs. 11 and 12 can be represented as a function of the phase lag set to a certain upper and lower bound limit, which in this case is set at 20%. This representation is a great way of determining the sensitivity of FDTR to the material parameters. Comparing Figs. 11b and 11c with Fig. 13a, the orange and yellow curves represent the sensitivity of FDTR to the in-plane and cross plane thermal conductivity of gold thin film.

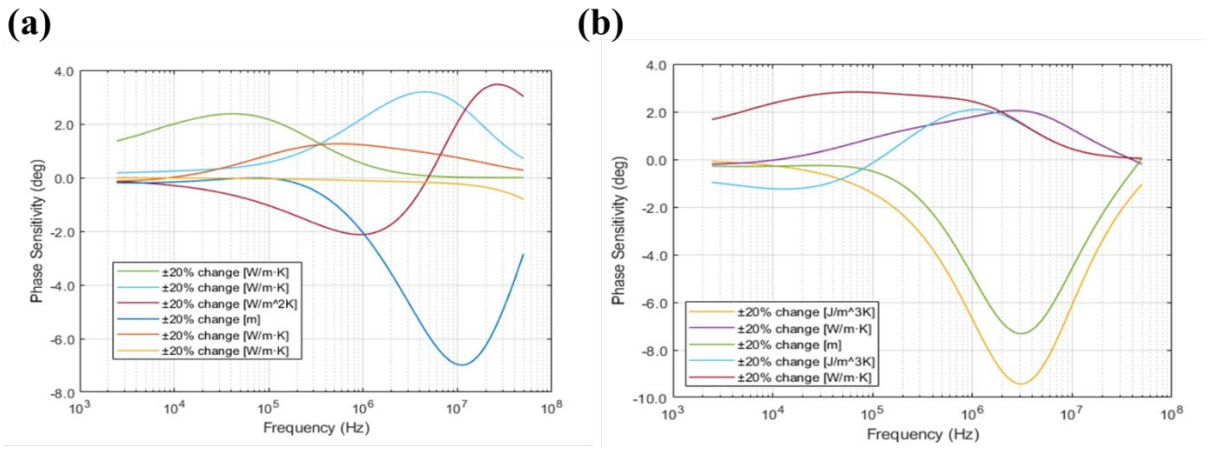

Figure 13. Sensitivity analysis of all the parameters of gold transducer and a) ZnSe and b) ZnTe as a function of phase change with limits of ±20% upper and lower bounds

The green and light blue curves in Figs. 13 corresponds to the FDTR's sensitivity to the in-plane and the cross plane thermal conductivity of ZnSe.

Analysis process similar to that of ZnSe was conducted for ZnTe as well in order to determine its thermal conductivity. Fig. 14 shows that with the help of accurately determined input parameters, we were able to achieve a good agreement between the FDTR's measurement of the

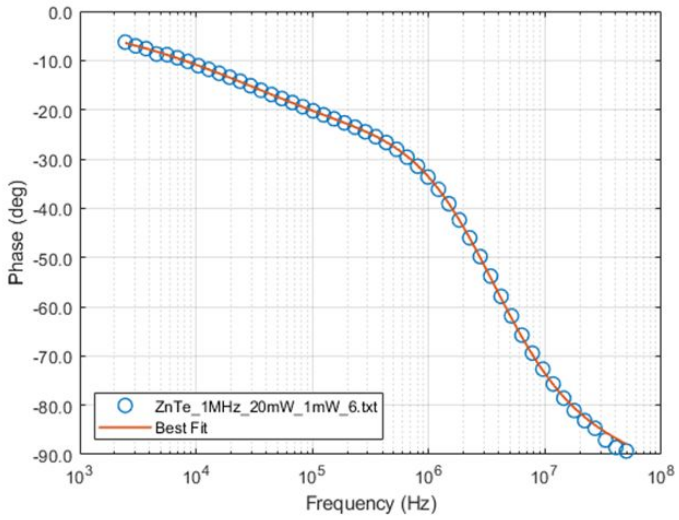

Figure 14. FDTR data for curve fitting analysis to calculate the thermal properties for ZnTe

phase lag and the phase lag calculated using the 2D diffusion model, keeping the thermal conductivity of ZnTe as a floating or a free parameter. This gives us a high confidence value of the thermal conductivity of ZnTe which was measured to be ~14 W/m-K.

Conclusion:

Using FDTR, the experimentally determined thermal conductivity values of natural occurring ZnSe and ZnTe are found to be ~17 W/m-K and 14 W/m-K respectively. These compare well to the computed results of around 23.2 W/m-K and 14.2 W/m-K for naturally occurring ZnSe and ZnTe respectively at 300K achieved using first-principles. The length dependent *k* value of ZnSe saw a significant reduction from 22.9 W/m-K to 1.8 W/m-K with the length scale diminishing from 10 μm to 10 nm. Similarly, for ZnTe, the *k* value was observed to decrease significantly from 12.6 W/m-K to 1.2 W/m-K with similar length scale reduction as ZnSe. The difference in the experimental and the computational results can be attributed to the dissimilarity in the polycrystallinity as obtained from the manufacturer and as modeled for computational analysis. FDTR can be utilized to measure the thermal properties of unknown material systems with great confidence and supplemented by the computational work, can allow a greater understanding of the physics of heat transport phenomena within material systems. Additionally, this combination of computational and experimental work using FDTR can allow tuning materials to achieve desired results for specific applications in the areas of thermal management and thermoelectric devices.

Conflicts of Interest

There are no conflicts of interest to declare.

Acknowledgements

RM, RSA, FT and JG acknowledge support from National Science Foundation award under Award No. #2115067. We also acknowledge OU Supercomputing Center for Education and Research (OSCER) for providing computing resources for this work.

References

1. Teepe, G. *The growing importance of microelectronics from a foundry perspective*. in *2014 Design, Automation & Test in Europe Conference & Exhibition (DATE)*. 2014. IEEE.
2. Austin, A.J., et al., *High-Temperature Atomic Layer Deposition of GaN on 1D Nanostructures.* Nanomaterials (Basel), 2020. **10**(12).
3. Qu, J., *8.06 - Thermomechanical Reliability of Microelectronic Packaging*, in *Comprehensive Structural Integrity*, I. Milne, R.O. Ritchie, and B. Karihaloo, Editors. 2003, Pergamon: Oxford. p. 219-239.

4. Moore, G.E., *Cramming more components onto integrated circuits.* Proceedings of the IEEE, 1998. **86**(1): p. 82-85.
5. Mandal, S., et al., *Atomic-Scale Insights on Large-Misfit Heterointerfaces in LSMO/MgO/c-Al2O3.* Crystals, 2021. **11**(12): p. 1493.
6. Muthaiah, R., et al., *First principles investigation of high thermal conductivity in hexagonal boron phosphide.* arXiv preprint arXiv:2201.09430, 2022.
7. Muthaiah, R., J. Garg, and S. Arafin, *Ultrahard BC5 – An efficient nanoscale heat conductor through dominant contribution of optical phonons.* Computational Materials Science, 2022. **206**: p. 111276.
8. Muthaiah, R., F. Tarannum, and J. Garg, *Strain tuned low thermal conductivity in Indium Antimonide (InSb) through increase in anharmonic phonon scattering-A first-principles study.* Solid State Communications, 2021. **334**: p. 114378.
9. Muthaiah, R. and J. Garg, *First principles investigation of high thermal conductivity in hexagonal germanium carbide(2H-GeC).* Carbon Trends, 2021. **5**: p. 100113.
10. Muthaiah, R. and J. Garg, *Thermal conductivity of magnesium telluride (MgTe)-A first principles study.* Solid State Communications, 2021. **337**: p. 114414.
11. Muthaiah, R. and J. Garg, *Thermal conductivity of magnesium selenide (MgSe)–A first principles study.* Computational Materials Science, 2021. **198**: p. 110679.
12. Muthaiah, R. and J. Garg, *Ultrahigh thermal conductivity in hexagonal BC6N- An efficient material for nanoscale thermal management- A first principles study.* Computational Materials Science, 2021. **200**: p. 110773.
13. Muthaiah, R. and J. Garg, *Strain tuned thermal conductivity reduction in Indium Arsenide (InAs)–A first-principles study.* Computational Materials Science, 2021. **196**: p. 110531.
14. Muthaiah, R., *THERMAL TRANSPORT IN POLYMERS, POLYMER NANOCOMPOSITES AND SEMICONDUCTORS USING MOLECULAR DYNAMICS SIMULATION AND FIRST PRINCIPLES STUDY.* 2021.
15. Muthaiah, R., et al., *Thermal conductivity of hexagonal BC2P – a first-principles study.* RSC Advances, 2020. **10**(70): p. 42628-42632.
16. Muthaiah, R. and J. Garg, *Strain tuned high thermal conductivity in boron phosphide at nanometer length scales – a first-principles study.* Physical Chemistry Chemical Physics, 2020.
17. Yang, L., N. Yang, and B. Li, *Reduction of thermal conductivity by nanoscale 3D phononic crystal.* Scientific reports, 2013. **3**(1): p. 1-5.
18. Due, J. and A.J. Robinson, *Reliability of thermal interface materials: A review.* Applied Thermal Engineering, 2013. **50**(1): p. 455-463.
19. Tian, Z., et al., *On the importance of optical phonons to thermal conductivity in nanostructures.* Applied Physics Letters, 2011. **99**(5): p. 053122.
20. Muthaiah, R. and J. Garg, *Strain tuned high thermal conductivity in boron phosphide at nanometer length scales – a first-principles study.* Physical Chemistry Chemical Physics, 2020. **22**(36): p. 20914-20921.
21. Kwon, O., L. Shi , and A. Majumdar, *Scanning Thermal Wave Microscopy (STWM).* Journal of Heat Transfer, 2003. **125**(1): p. 156-163.
22. Paddock, C.A. and G.L. Eesley, *Transient thermoreflectance from thin metal films.* Journal of applied physics, 1986. **60**(1): p. 285-290.
23. Capinski, W.S. and H.J. Maris, *Improved apparatus for picosecond pump-and-probe optical measurements.* Review of Scientific Instruments, 1996. **67**(8): p. 2720-2726.
24. Cahill, D.G., *Analysis of heat flow in layered structures for time-domain thermoreflectance.* Review of scientific instruments, 2004. **75**(12): p. 5119-5122.

25. Schmidt, A.J., R. Cheaito, and M. Chiesa, *A frequency-domain thermoreflectance method for the characterization of thermal properties.* Review of scientific instruments, 2009. **80**(9): p. 094901.
26. Ding, J., et al., *Thermoelectric transport properties in chalcogenides ZnX (X=S, Se): From the role of electron-phonon couplings.* Journal of Materiomics, 2021. **7**(2): p. 310-319.
27. Zhang, H. and Y. Fang, *Temperature dependent photoluminescence of surfactant assisted electrochemically synthesized ZnSe nanostructures.* Journal of Alloys and Compounds, 2019. **781**: p. 201-208.
28. Khan, T.M., et al., *Synthesis of thermally evaporated ZnSe thin film at room temperature.* Thin Solid Films, 2011. **519**(18): p. 5971-5977.
29. Lugueva, N.V., S.M. Luguev, and A.A. Dunaev, *Thermal conductivity of polycrystalline zinc selenide.* Physics of the Solid State, 2003. **45**(3): p. 449-452.
30. Chandramohan, R., C. Sanjeeviraja, and T. Mahalingam, *Preparation of Zinc Selenide Thin Films by Electrodeposition Technique for Solar Cell Applications.* physica status solidi (a), 1997. **163**(2).
31. Morkoç, H., et al., *Large-band-gap SiC, III-V nitride, and II-VI ZnSe-based semiconductor device technologies.* Journal of Applied Physics, 1994. **76**(3): p. 1363-1398.
32. Li, P. and T. He, *Recent advances in zinc chalcogenide-based nanocatalysts for photocatalytic reduction of CO2.* Journal of Materials Chemistry A, 2021. **9**(41): p. 23364-23381.
33. Langer, D.W. and C.J. Vesely, *Electronic Core Levels of Zinc Chalcogenides.* Physical Review B, 1970. **2**(12): p. 4885-4892.
34. Gangadharan, R., et al., *Electronic and structural properties of zinc chalcogenides ZnX (X= S, Se, Te).* Journal of alloys and compounds, 2003. **359**(1-2): p. 22-26.
35. Sun, Y., et al., *Fabrication of flexible and freestanding zinc chalcogenide single layers.* Nature Communications, 2012. **3**(1): p. 1057.
36. Davami, K., et al., *Thermal conductivity of ZnTe nanowires.* Journal of Applied Physics, 2013. **114**(13): p. 134314.
37. Sun, Y., et al., *Fabrication of flexible and freestanding zinc chalcogenide single layers.* Nature communications, 2012. **3**(1): p. 1-7.
38. Broido, D., L. Lindsay, and T. Reinecke, *Ab initio study of the unusual thermal transport properties of boron arsenide and related materials.* Physical Review B, 2013. **88**(21): p. 214303.
39. Broido, D.A., et al., *Intrinsic lattice thermal conductivity of semiconductors from first principles.* Applied Physics Letters, 2007. **91**(23): p. 231922.
40. Garg, J., et al., *Role of Disorder and Anharmonicity in the Thermal Conductivity of Silicon-Germanium Alloys: A First-Principles Study.* Physical Review Letters, 2011. **106**(4): p. 045901.
41. Haynes, W.M., *CRC Handbook of Chemistry and Physics*. 2011: CRC Press.
42. Casimir, H.B.G., *Note on the conduction of heat in crystals.* Physica, 1938. **5**(6): p. 495-500.
43. Regner, K., S. Majumdar, and J.A. Malen, *Instrumentation of broadband frequency domain thermoreflectance for measuring thermal conductivity accumulation functions.* Review of Scientific Instruments, 2013. **84**(6): p. 064901.
44. Zhu, J., et al., *Ultrafast thermoreflectance techniques for measuring thermal conductivity and interface thermal conductance of thin films.* Journal of Applied Physics, 2010. **108**(9): p. 094315.
45. Yang, J., C. Maragliano, and A.J. Schmidt, *Thermal property microscopy with frequency domain thermoreflectance.* Review of Scientific Instruments, 2013. **84**(10): p. 104904.
46. Yang, J., *Thermal property measurement with frequency domain thermoreflectance*. 2016, Boston University.
47. Qian, X., et al., *Accurate measurement of in-plane thermal conductivity of layered materials without metal film transducer using frequency domain thermoreflectance.* Review of Scientific Instruments, 2020. **91**(6): p. 064903.

48. Jiang, P., X. Qian, and R. Yang, *A new elliptical-beam method based on time-domain thermoreflectance (TDTR) to measure the in-plane anisotropic thermal conductivity and its comparison with the beam-offset method.* Review of Scientific Instruments, 2018. **89**(9): p. 094902.
49. Feser, J.P., J. Liu, and D.G. Cahill, *Pump-probe measurements of the thermal conductivity tensor for materials lacking in-plane symmetry.* Review of Scientific Instruments, 2014. **85**(10): p. 104903.
50. Li, M., J.S. Kang, and Y. Hu, *Anisotropic thermal conductivity measurement using a new asymmetric-beam time-domain thermoreflectance (AB-TDTR) method.* Review of Scientific Instruments, 2018. **89**(8): p. 084901.
51. Liu, J., et al., *Simultaneous measurement of thermal conductivity and heat capacity of bulk and thin film materials using frequency-dependent transient thermoreflectance method.* Review of Scientific Instruments, 2013. **84**(3): p. 034902.
52. Wei, C., et al., *Invited Article: Micron resolution spatially resolved measurement of heat capacity using dual-frequency time-domain thermoreflectance.* Review of Scientific Instruments, 2013. **84**(7): p. 071301.
53. Wilson, O.M., et al., *Colloidal metal particles as probes of nanoscale thermal transport in fluids.* Physical Review B, 2002. **66**(22): p. 224301.
54. Schmidt, A., et al., *An optical pump-probe technique for measuring the thermal conductivity of liquids.* Review of Scientific Instruments, 2008. **79**(6): p. 064902.
55. Schmidt, A.J., R. Cheaito, and M. Chiesa, *Characterization of thin metal films via frequency-domain thermoreflectance.* Journal of Applied Physics, 2010. **107**(2): p. 024908.
56. Costescu, R.M., M.A. Wall, and D.G. Cahill, *Thermal conductance of epitaxial interfaces.* Physical Review B, 2003. **67**(5): p. 054302.
57. Luckyanova, M.N., et al., *Coherent phonon heat conduction in superlattices.* Science, 2012. **338**(6109): p. 936-939.
58. Lyeo, H.-K. and D.G. Cahill, *Thermal conductance of interfaces between highly dissimilar materials.* Physical Review B, 2006. **73**(14): p. 144301.
59. Hopkins, P.E., et al., *Manipulating thermal conductance at metal–graphene contacts via chemical functionalization.* Nano letters, 2012. **12**(2): p. 590-595.
60. Hopkins, P.E., et al. *Effects of surface roughness and oxide layer on the thermal boundary conductance at aluminum/silicon interfaces*. in *International Heat Transfer Conference*. 2010.
61. Yang, J., et al., *Thermal conductance imaging of graphene contacts.* Journal of Applied Physics, 2014. **116**(2): p. 023515.
62. Paulatto, L., et al., *First-principles calculations of phonon frequencies, lifetimes, and spectral functions from weak to strong anharmonicity: The example of palladium hydrides.* Physical Review B, 2015. **91**(5): p. 054304.
63. Paulatto, L., F. Mauri, and M. Lazzeri, *Anharmonic properties from a generalized third-order ab initio approach: Theory and applications to graphite and graphene.* Physical Review B, 2013. **87**(21): p. 214303.
64. Fugallo, G., et al., *Ab initio variational approach for evaluating lattice thermal conductivity.* Physical Review B, 2013. **88**(4): p. 045430.
65. Giannozzi, P., et al., *QUANTUM ESPRESSO: a modular and open-source software project for quantum simulations of materials.* Journal of Physics: Condensed Matter, 2009. **21**(39): p. 395502.
66. Ceperley, D.M. and B.J. Alder, *Ground State of the Electron Gas by a Stochastic Method.* Physical Review Letters, 1980. **45**(7): p. 566-569.

67. Monkhorst, H.J. and J.D. Pack, *Special points for Brillouin-zone integrations.* Physical Review B, 1976. **13**(12): p. 5188-5192.
68. Garg, J., N. Bonini, and N. Marzari, *First-Principles Determination of Phonon Lifetimes, Mean Free Paths, and Thermal Conductivities in Crystalline Materials: Pure Silicon and Germanium*, in *Length-Scale Dependent Phonon Interactions*, S.L. Shindé and G.P. Srivastava, Editors. 2014, Springer New York: New York, NY. p. 115-136.
69. Jiang, P., X. Qian, and R. Yang, *Tutorial: Time-domain thermoreflectance (TDTR) for thermal property characterization of bulk and thin film materials.* Journal of Applied Physics, 2018. **124**(16): p. 161103.
70. Hao, Q., Y. Xiao, and Q. Chen, *Determining phonon mean free path spectrum by ballistic phonon resistance within a nanoslot-patterned thin film.* Materials Today Physics, 2019. **10**: p. 100126.
71. Hao, Q. and J. Garg, *A review on phonon transport within polycrystalline materials.* ES Materials & Manufacturing, 2021.
72. https://www.mtixtl.com/crystalssubstratesa-z.aspx.